Influence of the self-excited induction generator in the improvement of the energy efficiency in isolated PAT systems

Caeiro, João Francisco
jonas.f.caeiro.@gmail.com
Instituto Superior Técnico
Lisbon, Portugal

ABSTRACT

The substitution of the pressure reducing valves (PRV) with Pump working as a Turbine (PAT) have been considered in the past years for being a viable solution as it provides both pressure control and energy savings, at a reasonable low price.

The using of PAT was identified by many researchers as a way to improve the energy efficiency in the water systems. However, most of the researches consider the hydraulic machine connected to the electrical grid, which may be inconvenient when these recovery systems are located in rural or remote areas. To improve the knowledge of the efficiency in these recovery systems for rural areas, this research contributes for a further study and optimization of the off-grid PAT systems with induction generators (IG). This thesis proposes a methodology to obtain the best optimization of PAT – SEIG (Self-excited Induction Generator) system while operating under different speeds and loads. Here, it can be found a proper solution considering the variation of the electrical parameters of the IG in order to maximize the energy efficiency also considering capacitor selection. Special attention is given to the possible impact of the SEIG parameters in optimizing the recovery system. These results showed increase accuracy for modeling the SEIG as an analytical model and simulation model.

Keywords: Energy efficiency, Self- Excited Induction Generator (SEIG), Pump working as a Turbine (PAT

1. Introduction

The uprising of energy consumption that has been seen throughout the last 20 years has criated the necessity for finding new and better alternatives for energy sources. In this context, investments were made in many renewable energy sources with small environmental impact, including in hydroelectric power generation, throughout the years.

Being the hydroelectric power generation a technology that has not change much in the last 20 years, there has been a peak interest in developing it. For this purpose, there has been a higher interest in studying small and micro-hydro solutions, being developed in areas where the electrical grid is not easily accessed. In this context, the installation of micro-hydro power source able to generate and store energy is a good alternative, however in certain cases it revealed some problems related with costs, due to the need to miniaturize the turbine. With this constraint in mind, a proposed solution was the use of a pump running in turbine mode (PAT), which represents a high reduction in the implementation costs. Although it may not be as efficient alternative as a hydro-turbine, it is considered to be an efficient method of generating energy, having some advantages such as a simple construction and durability

2. Induction Machine and its electrical parameters

2.1 Problem found and proposed solution

The values of the capacitance required to excite the SEIG were analysed by (Capelo *et al.*, 2017) and these values were calculated for different resistive loads and for different rotational speeds of the DC motor that represents the hydraulic machine in the electric experiments. This "off-grid" recovery system is an interesting topic to study but in this study, there was some assumptions that can be dangerous for the machine. The assumption was to not consider the iron losses in the machine, represented by R_m and assume that all the electrical induction generator parameters remain time invariant for different rotational speeds and for different levels of magnetization ($\frac{E}{f}$)

A solution was proposed. It will be necessary to determine if the capacitance values required to excite the SEIG in (Capelo, 2017) were accurately estimated. And so, it was required a brief study of the induction generator and its variation of the electrical parameters.

Figure 2.1 shows us an equivalent of an induction machine with its electrical parameters:

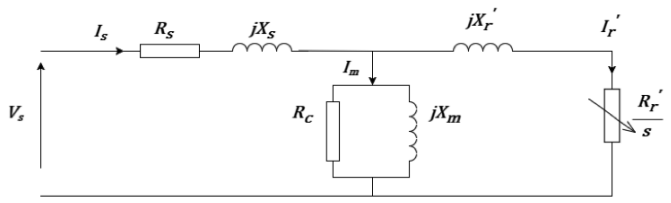

Figure 2-1 – Electrical equivalent of an induction machine

The electrical equivalent circuit from figure 2.1 can be divided into three different parts: stator, magnetization and rotor. The resistance R_S represents the resistance of the stator winding and X_S represents the stator leakage reactance. The resistance R_C represents the core losses and X_m represents the magnetization reactance. Finally, for the rotor side, X_r and $\frac{R_r}{s}$ represent the rotor's reactance and resistance, respectively

Figure 2.2 represents the induction generator that was used for this study and its rated values are shown in Table 2.1. This machine has a rated efficiency of $\eta_N = 68\%$ and a nominal slip of $s_N = 9\%$.

Figure 2-2 – Induction machine used for experimental tests

Table 2.1 - Nameplate data of the induction machine

3 – phase induction machine	
Frequency	50 Hz
Voltage	400V
Current	1.6A
Output Power	0,55 KW
Power Factor	0.73
Speed	910 rpm

2.2 Blocked Rotor and no-load tests

After knowing and studied the machine, there is now the need to study its behavioral effect when faced with non-normal conditions, which are variation frequency and different levels of magnetization with different applied voltages.

Figure 2.3 shows a diagram of the experimental set-up. In this set-up, the induction machine was powered by an isolated salient-pole synchronous generator driven by a DC motor. Using this approach, the DC motor speed will apply the electrical frequency in the system and synchronous generator excitation will set the induction motor voltage applied to the induction machine

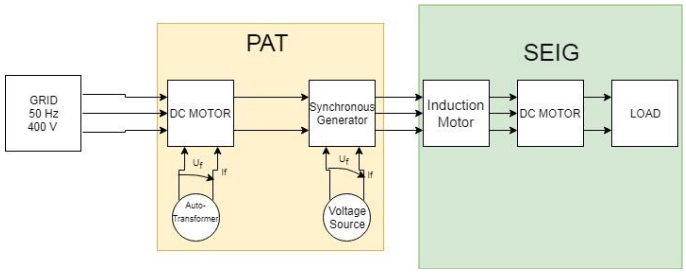

Figure 2-3 - Diagram of the experimental tests for the behavior of the induction machine

To determine the parameters of the machine it was necessary to perform two tests: Blocked rotor and no-load. It was imposed a three-phase stator voltage having different amplitude and frequency. These tests were done for frequency between 20 and 60 Hz, with 10 Hz intervals. For each frequency, different voltages were applied to the induction machine, but never exciding more than 20% of its nominal current. The range of frequencies was selected based upon SEIG operation on previous work (Capelo, 2017) For each test the voltage and current values of the induction and also each phase active and reactive power with its power factor were measured. The rotor speed was acquired as well as the electrical frequency and the applied voltage in the machine.

The blocked rotor test is where the rotor axis of the machine and so the induction machine does not rotate and because there are no induced currents in the stator, the magnetization branch is neglected. Figure 2.4 is an equivalent electrical circuit for blocked rotor:

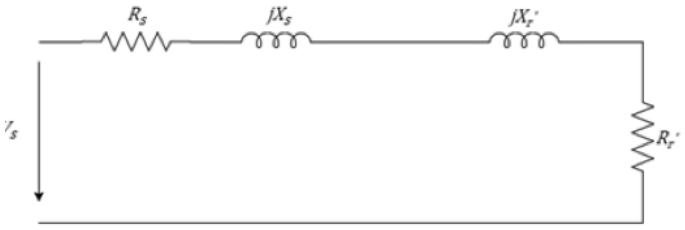

Figure 2-4 - Equivalent circuit of blocked rotor test, adapted from (Paiva, 2011)

In order to obtain the stator and rotor inductances (X_s and X_r') as well as the rotor resistance (R_r') the equivalent electrical system has to be studied. In order to do that we have to use the equations (3.1) – (3.3) are used.

$$Q_{sc} = S_{sc} * \sin\varphi \quad (2.1)$$

$$R = R_s + R_r' = \frac{P_{sc}}{I_{sc}^2} <=> \frac{P_{sc}}{I_{sc}^2} - R_s = R_r \quad (2.2)$$

$$X = X_s + X_r{}' = \frac{Q_{sc}}{I_{sc}{}^2} \quad (2.3)$$

The no-load test, like the open circuit test on a transformer, gives information about exciting current and rotational losses (Paiva, 2011). The machine will rotate at almost a synchronous speed, which makes slip nearly zero. Figure 2.5 show the no-load equivalent of induction machine is again simplified. However, this time the secondary branch is the one to be neglected.

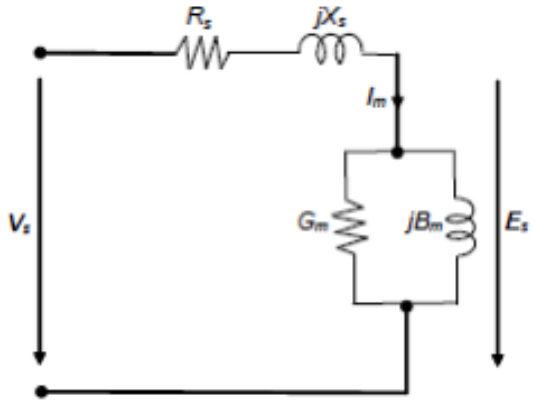

Figure 2-5 - Equivalent circuit for the no-load test adapted from (Paiva, 2011)

Figure 2.5 represents the magnetizing parameters by $G_m and\ B_m$. However, this thesis considers G_m as R_m and B_m as X_m . Equations 2.4 and 2.5 determines the magnetizing electrical parameters:

$$R_m = G_m = \frac{U_{0avg}{}^2}{(P_{0avg} - I_{0avg}{}^2 * R_s)} \quad (2.4)$$

$$X_m = B_m = \frac{U_{0avg}{}^2}{(Q_{0avg} - I_{0avg}{}^2 * X_s)} \quad (2.5)$$

2.3 Results Analysis

The results for the tests are represented in figures 2.6, 2.7, 2.8 and 2.9. It was only used the data from the tests and the figures shows the parameters as the function of the magnetizing levels. Figures 2.6 and 2.7 shows the results for the blocked rotor. For the stator resistance, R_S, it was measured and for every test it remained constant ($R_S = 18.8\Omega$)

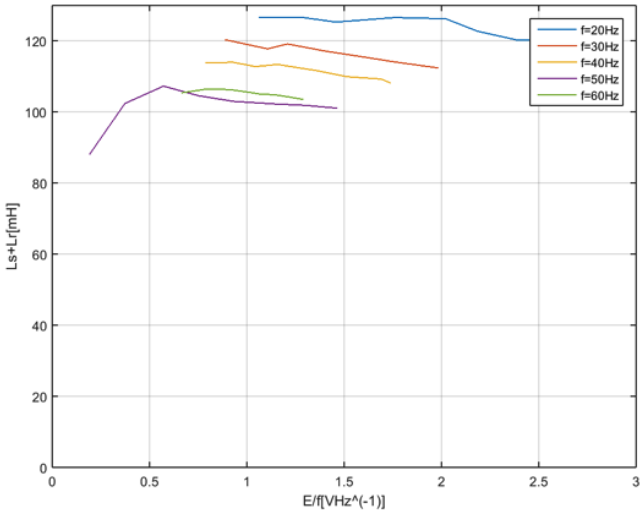

Figure 2-6 - Behavior of the rotor and stator inductance through magnetization levels

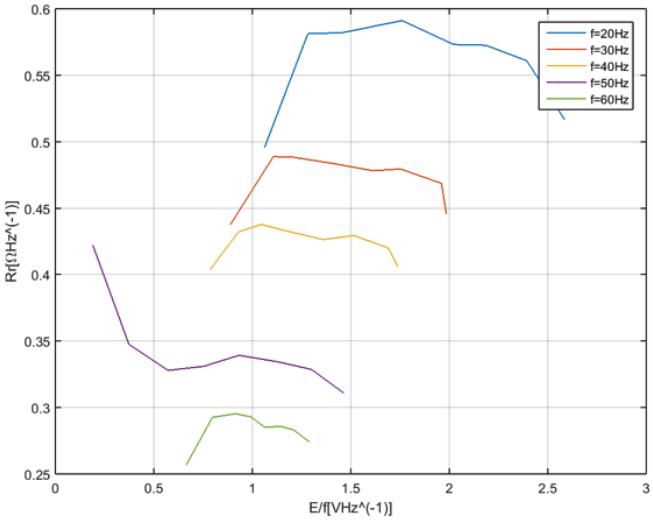

Figure 2-7 - Behavior of the rotor resistance through magnetization level

Figure 2.6 show the sum of total and rotor leakage inductance. These values are between 0.10H and 0.13 H and it shows that these values are independent for any magnetization level (E/f) of the generator and it was considered from now on that rotor and stator leakage is a fixed parameter with a value of 0.055H each.

Figure 2.7 represents the rotor resistance behavior through the applying of different magnetization levels. It is seen that this parameter does not change that much with different magnetization and that can be explained with the next equations(Fernandes *et al.*, 2018):

$$E = [R_{'r} + (j2\pi f L_{'r})]I_{'r} \quad (2.6)$$

This is the magnetomotive force created induced in the rotor. By dividing all the parameters with the frequency, we get the variation of the magnetization levels with the two rotor parameters.

$$\frac{E}{f} = [\frac{R'_r}{f} + (j2\pi L_{'r})]I_r \quad (2.7)$$

This can show that for any increase of the magnetization value, there is a proportional increase in the rotor current, which means that both R'_r and $L_{'r}$ remain approximately constant with the magnetization level.

Figure 2.8 and 2.9 show now the results for the no-load test and in them there are the behavior of the magnetizing parameters.

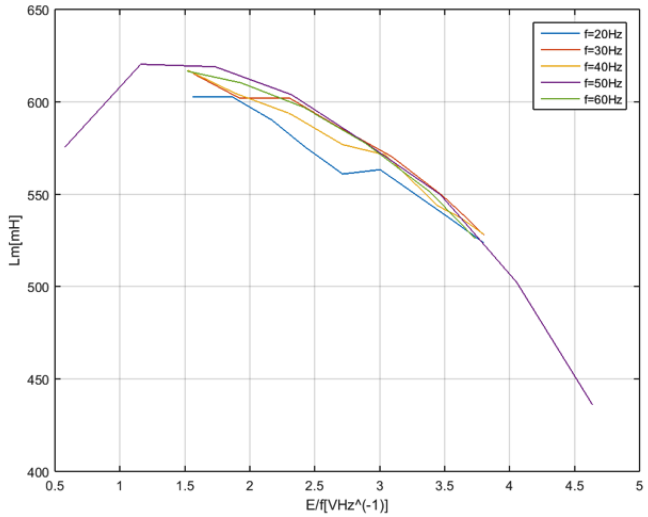

Figure 2-8 - Evolution of the Magnetic Inductance

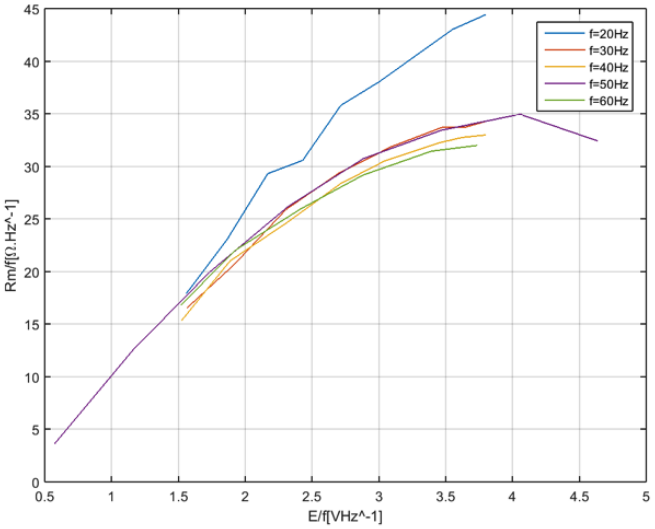

Figure 2-9 - Evolution of the Core losses

The magnetizing inductance, L_m, is a function of the magnetization level. Using the nameplate data of the induction machine in Table 2.1, the nominal level of magnetization per phase is $\frac{230}{50} = 4.6\,V.Hz^{-1}$, What is seen in figure 2.8 is that there is a point that the remains stable. This is seen from $E/V = 1\ to\ E/V = 2$. This is explained because the machine is design to work on the linear B-H curve. For higher values of the magnetization level there is a decrease of the magnetizing inductance because now the generator stars to operate on the saturated curve, which means for every increase of $B = \frac{E}{f}$ the magnetic field stays the same and the magnetization decreases.

At last, Figure 2.9 shows the evolution of the magnetization resistance R_m divided by the electrical frequency, *f*, as a function of the magnetization level, *E/f*. Independent of the electric frequency, R_m increases as the magnetizing flux in the generator increases. The power losses in the magnetization resistance are associated with iron losses due to the eddy current and the hysteresis effect. Equation 2.8 is the computation of these power losses as a function of these two physical phenomena.

$$P_m = k_h * (\frac{E}{f}) * f + k_e(\frac{E}{f}) * f^2 = P_h + P_e \quad (2.8)$$

As It is known the effect of the hysteresis is much higher than the eddy currents, so it is possible to neglect P_e. By manipulating (2.8) it is obtained(Fernandes *et al.*, 2018):

$$P_m = \frac{E^2}{R_m} = \frac{E^2}{f}\frac{f}{R_m} = k_h\left(\frac{E}{f}\right)f \quad (2.9)$$

$$E\frac{f}{R_m} = k_h f \quad (2.10)$$

$$\frac{R_m}{f} = \frac{E}{k_h f} \quad (2.11)$$

With these results it can be concluded that both primary and secondary branches does not get affected by the magnetization levels however the electrical parameters are highly affected with the magnetization.

To conclude, and in order to further this research, there is the assumption that all the electrical parameters can be fixed as a constant rated value except for the magnetization branches that are going to be variable in the determination of an analytical and Simulation Model.

3. SEIG: Analytical and Simulation Model

3.1 Analytical Model

Although the analytical methodology follows the same steps that were presented in [1], it is now included the iron losses in the induction generator equivalent circuit. The Figure 3.1 represents the SEIG system. SEIG system is divided into three main nodes: induction generator, load and capacitance. As it was made in [1] it is going to be applied the Nodal Admittance Approach, where we determine our equations through the main nodes in the system. This is the easiest approach that facilitates the calculations due to the fact that parallel admittances sum to each other while determine the total admittance of some system

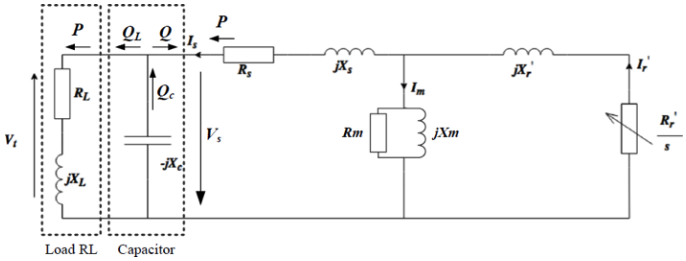

Figure 3-1 - Equivalent electric circuit of the self-excited induction generator connected to the load [(Fernandes *et al.*, 2018)]

The equivalent electric circuit can be furthermore reduced to its per-unit values by dividing all parameters by the per-unit frequency, $a = \frac{f}{f_N}$[4]. For an electrical quantity, the frequency can be expressed as $f = a.f_N$

All the electrical parameters should now be divided by a in order for everyone be normalized under the same per-unit frequency.

$$\frac{X_S}{a} = 2\pi f_N L_s = X_{s_N} \quad (3.1)$$

$$\frac{X_r}{a} = 2\pi f_N L_r = X_{r'_N} \quad (3.2)$$

$$\frac{X_m}{a} = 2\pi f_N L_m = X_{m_N} \quad (3,3)$$

$$\frac{X_L}{a} = 2\pi f_N L_L = X_{L_N} \quad (3.4)$$

$$\frac{X_c}{a} = \frac{1}{2\pi a^2 f_N C} = \frac{X_{C_N}}{a^2} \quad (3.5)$$

Now with the help of the nodal Admittance approach and the help of the Kirchhoff current Law we can compute the total admittance of the system:

$$\frac{V_t}{a} \times Y_t = 0 \quad (3.6)$$

$$Y_t = Y_{IN} + Y_L + Y_C \quad (3.7)$$

In order to assure the self-excitation of the induction generator, the total admittance of equivalent circuit must be zero. This is the same step that is used in [(Capelo *et al.*, 2017)] however there is now the use of the iron losses parameter R_m. The total admittance is the parallel association between Load, capacitor and induction generator. The series of equations from (3.8) to (3.13) sets the admittances of rotor, stator, magnetizing branches, induction generator, load and capacitance.

$$Y_C = -\frac{a^2}{jX_C} \quad (3.8)$$

$$Y_L = \frac{1}{\frac{R_L}{a} + jX_L} \quad (3.9)$$

$$Y_m = \frac{1}{\frac{R_m}{a}} + \frac{1}{jX_m} = \frac{a}{R_m} - \frac{j}{Xm} \quad (3.10)$$

$$Y_r = \frac{1}{\frac{R_r'}{a} + jX_r'} \quad (3.11)$$

$$Y_s = \frac{1}{\frac{R_s}{a} + jX_s} \quad (3.12)$$

$$Y_{in} = \frac{Ys(Yr+Ym)}{Ys+Yr+Ym} \quad (3.13)$$

Then it is necessary to separate the total admittance into real and imaginary part in order to determine the electrical frequency and the minimal capacitance values.

$$Re\{Y_t\} = 0 \quad (3.14)$$

$$Im\{Y_t\} = 0 \quad (3.15)$$

Equation 3.14 does not have a parameter that is directly influenced by the per-unit frequency and so this equation its chosen for the determination of the per-unit frequency values, a_k. Then, these values are going to be used in the equation 3.15 to determine the minimal capacitance inductance that excites the SEIG induction machine. Equation (3.16), (3.17) and (3.18) represents the determination of the per unit frequency from eq 3.14, the determination of the capacitance inductance from equation 3.15 and the determination of the minimal capacitance required to excite the SEIG, respectively.

$$D_6a^6 + D_5a^5 + D_4a^4 + D_3a^3 + D_2a^2 + D_1a^1 + D_0 = 0 \quad (3.16)$$

$$X_{C_N} = -\frac{A_8a^8 + A_7a^7 + A_6a^6 + A_5a^5 + A_4a^4 + A_3a^3 + A_2a^2 + A_1A + A_0}{B_6a^6 + B_5a^5 + B_4a^4 + B_3a^3 + B_2a^2 + B_1a + B_0} \quad (3.17)$$

$$C_k = \frac{1}{2\pi f_N a_k X_{C_N}}, \; k = 1, \ldots, 8 \quad (3.18)$$

Note that from (Capelo, 2017) there were 4 possible determination of the per-unit frequency value. Now due to the inclusion of the iron losses there are now 6 possible values for the frequency.

These calculations are not a linear process because the parameters of the induction generator may change for different operating points. Thus, it is important to elaborate an advanced version of the previous analytical methodology capable of including the change of machine parameters according its operating point.

3.1.1 MatLab Analytical Model Data

To compute the electrical parameters, the voltage and electrical frequency of the machine, which depends on the electrical parameters, must be known. To understand better what was made in the MatLab calculations a flowchart of the code is shown in Figure 3.3. In this model, the electrical reactance must be defined at the rated frequency of the induction generator.

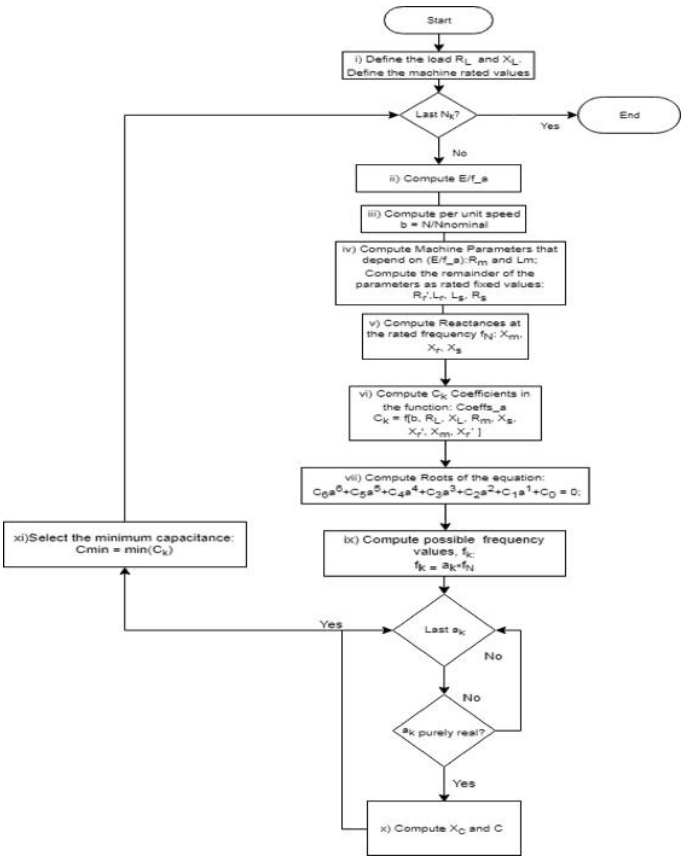

Figure 3-2 - Flowchart of the Matlab analytical Model

The algorithm starts in step (i) where the load electrical parameters (i.e., R_L and X_L) are defined. After determining the range of different speeds that the generator will operate, a cycle commences where steps from ii) to xi) are repeated the method converge for the speed value. This cycle keeps running until all the range of speeds are swept. The cycle starts in step ii) where it is computed the rated magnetic flux of the machine, with $\frac{E}{f\_0}$. Then through steps iii) to ix) are made the needed requirements to find all the six possible frequencies. Step iii) is where is determined the per unit speed, $b\ [p.u.]$, and through steps iii) to v) the electrical parameters of the SEIG are computed, namely the parameters R_m and L_m with their dependence upon the rated magnetization $\frac{E}{f\_a}$. in step iv) The remaining parameters are considered constant at their rated values. Step vi) is necessary to determine the coefficients of the equation (4.20) as step vii) is where the algorithm determines the roots of step vi). After that the algorithm calculates all the six frequencies that could possibly be used in the computation of the X_C and the $Cmin$. Having all the six frequencies been calculated is time to enter a new cycle within the cycle where now is these frequencies that are going to be swept. Before step x), there is a logical test to be passed and it is if the frequencies are purely real. With the last of those it is now possible to calculate X_C and C. After passing this cycle, it is determined the least Capacitance available.

3.1.2 MatLab Model Reults

In the next two figures there has been made a comparison between the minimal capacitance values obtained in (Capelo, 2017) and the values that are obtained now in this work.

From figures (3.4) to (3.6) it is seen that the minimal capacitances in the analytical model, where there was no regard towards the core losses, all the capacitors were over dimensioned. This is extremely important because every time there is an experimental work where the analytical model did not consider the core losses, the machine is working above the nominal conditions. The data from the three resistances shows that the capacitance was overestimated, which might affect the longevity and well-functioning of the IG in future researches. This is an important conclusion to consider for the safety of the machine and for the costs of an Off-grid PAT+SEIG application.

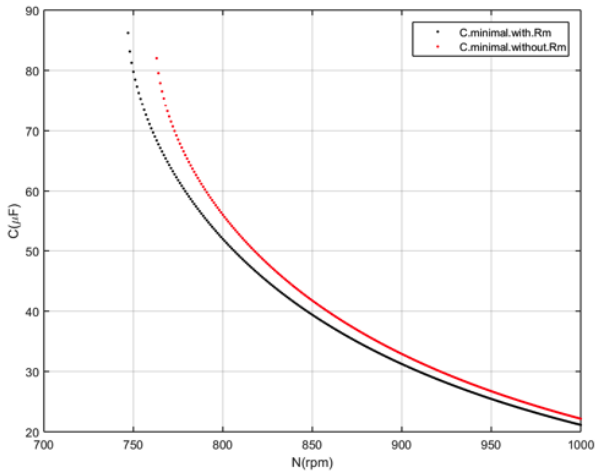

Figure 3-3 - Required minimal capacitances for exciting a SEIG for RL=600 Ω

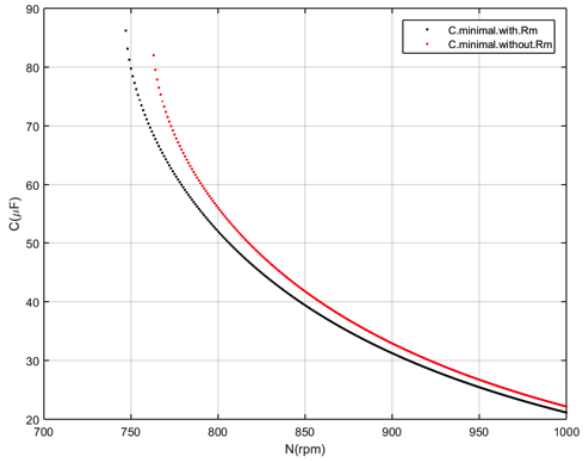

Figure 3-4 - Required minimal capacitances for exciting a SEIG for RL=300 Ω

3.2 Simulation Model

In this section it is going to be simulated the SEIG machine with a creation of a proper Simulink simulation model which has the objective of recreating the environment of an Off-Grid SEIG scenario with the most possible accuracy.

The simulation model Is represented in figure 3.7 where it observed 4 blocks: Mechanical equation, Load, capacitor and induction machine.

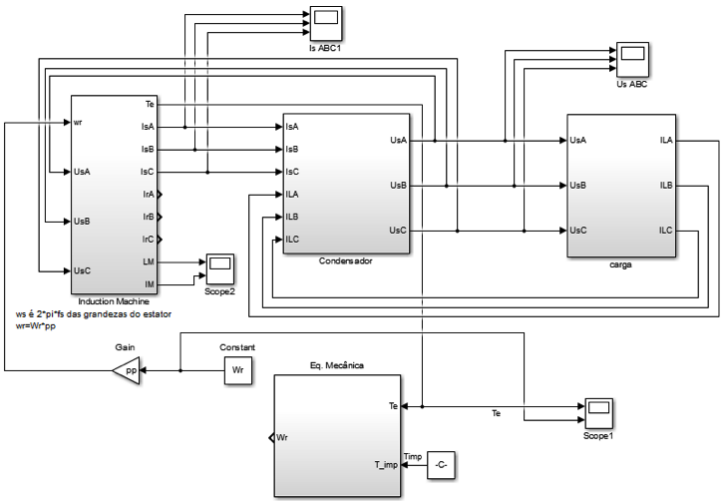

Figure 3-5 - SEIG SImulink Model

The load block is modeled by the following equation (Kishore and Kumar, 2006)

$$i_{L_k} = \int \frac{1}{L} U_{s_k} - \frac{R}{L} i_{L_k}.\ k = A, B, C \qquad (3.19)$$

From figure 3.7, under the alias "*carga*", it is seen the three inputs of the load block, the three phases of the Stator voltages, as well as three outputs, the three phases of the load current. Figure 3.8 shows the load block developed in Simulink and three equations, $i_{L_A}, i_{L_B}, i_{L_C}$, that determine the load current.

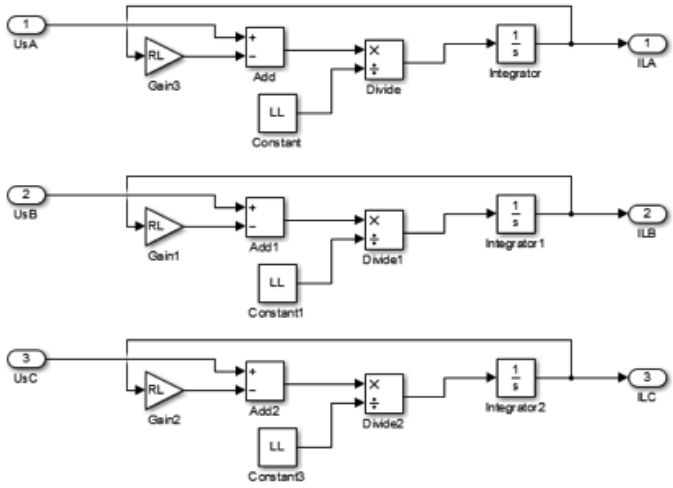

Figure 3-6 - Load Simulink Block Model

The excitation block is also a block with three equations, for each phase, where the inputs are the stator currents and the load currents that were developed in the load block. The outputs are the three phase stator voltages that goes into both load and induction generator blocks. These equations were presented by (Kishore and Kumar, 2006) during the work about a determination of a model of an off-grid SEIG using Space State approach.

$$U_{L_k} = \int \frac{1}{C} i_{s_k} - \frac{1}{C} i_{L_k}, \quad k = A, B. C \tag{3.20}$$

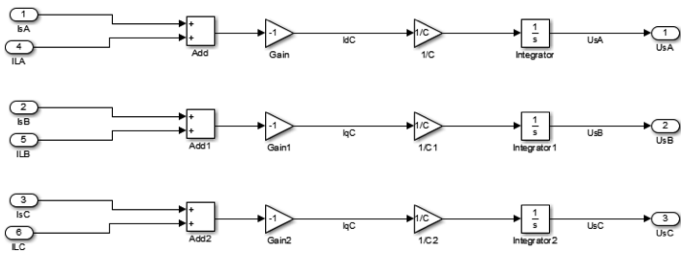

Figure 3-7 - Load block Simulink diagram

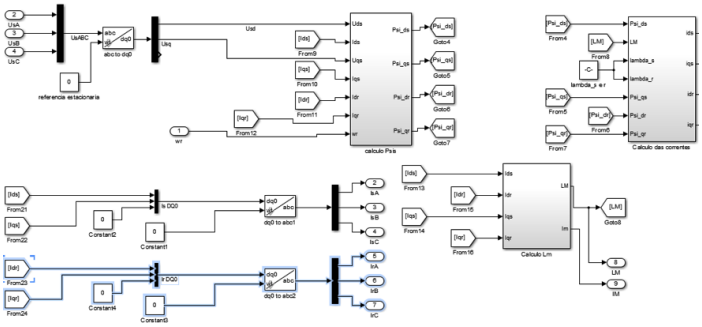

Figure 3-8 - Induction generator block

The Simulink induction generator block represented in figure 3.7 has 4 outputs, the 3 phases of the stator voltage and the rotational speed, and has 9 outputs, the 3 phases of the rotor and stator currents, the electromagnetic torque and both the magnetic induction and the magnetization current.

The computation for the magnetic flux, rotor and stator current are made in the equations below.

$$\psi_{d_s} = \int Ud_s - R_s i_{d_s} \tag{4.50}$$

$$\psi_{q_s} = \int Uq_s - R_s i_{q_s} \tag{4.51}$$

$$\psi_{d_r} = \int U_{d_r} - i_{d_r} * r_r + w_r * \psi_{q_r} \tag{4.52}$$

$$\psi_{q_r} = \int U_{q_r} - i_{q_r} * r_r + w_r * \psi_{d_r} \tag{4.53}$$

$$i_{d_s} = \frac{\psi_{d_s} - L_m * i_{d_r}}{L_s} \tag{4.54}$$

$$i_{q_s} = \frac{\psi_{q_s} - L_m * i_{q_r}}{L_s} \tag{4.55}$$

$$i_{d_r} = \frac{\psi_{d_r} - L_m * i_{d_s}}{L_r} \tag{4.56}$$

$$i_{q_r} = \frac{\psi_{q_r} - L_m * i_{q_s}}{L_r} \tag{4.57}$$

3.2.1 Simulation Results

This simulation allows obtaining three different graphs:

- The three phases of the Stator voltage:
- The three phases of the Stator current;
- The electrical torque and the rotational speed of the machine;

To compare the values between the experimental capacitance values many simulations were performed. For three different purely resistive loads of 120, 200 and 600 ohms, the model was simulated for different speeds and different capacitances. For a defined speed, it would be necessary to run some more simulations until it was found the smallest capacity possible in order the machine to start and for the output of stator current reached its nominal value of 1.6A. Although it is not being compared the smallest capacity possible, the capacitance value that were taken into consideration are like those ones, sometimes the difference of some μF.

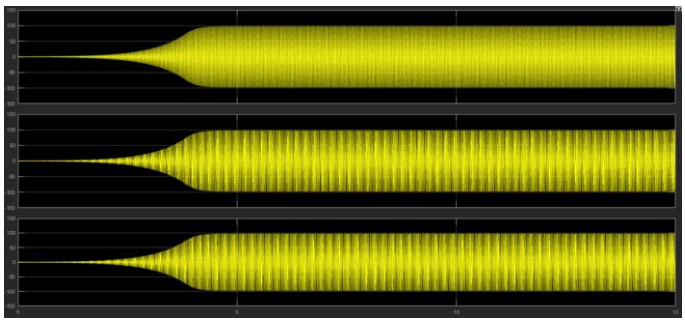

Figure 3-9 - Stator voltage results for a resistance of $R = 120\,\Omega$ and an excitation of $C = 58\mu F$ and for a time range of 15 seconds

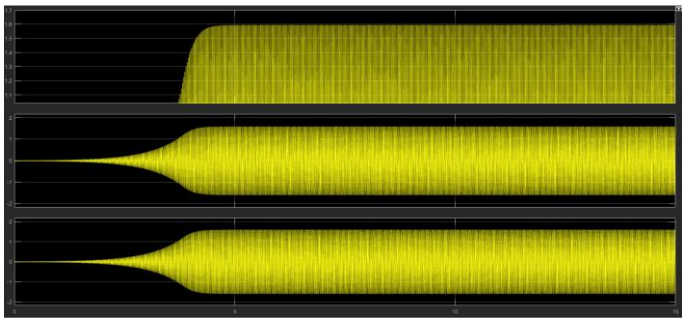

Figure 3-10 - Stator current results for a resistance of $R = 120\Omega$ and an excitation of $C = 58\mu F$ and for a time range of 15 seconds.

3.3 Experimental Work

To analyze the behavior of the SEIG, an experimental system was assembled in the Electrical Machines Laboratory. The objective of these experimental tests was to analyze the performance of a SEIG and to determine the minimal required capacitance to make the SEIG work under nominal conditions. It is also considered a comparison between the determined capacitances in the simulation tests and the real

capacitances, in order to validate the simulation model. Finally, it is also assessed the capacitor bank influence on the system.

3.3.1 Test and Results

The flowchart of the figure 3.11**Erro! A origem da referência não foi encontrada.** shows the sequence of the tests performed. For a load value, it is applied a constant current I_f and voltage V_f in the DC moor field circuit. It was done with the help of the DC power source in the bench and a variable resistor, which regulated the necessary field current ($0.51\,A$). Then with the help of a three-phase autotransformer, that has the goal of regulating the 3-phase voltage that comes from the grid (230 V, 50Hz) in order to regulate the speed of the DC Motor-SEIG system.

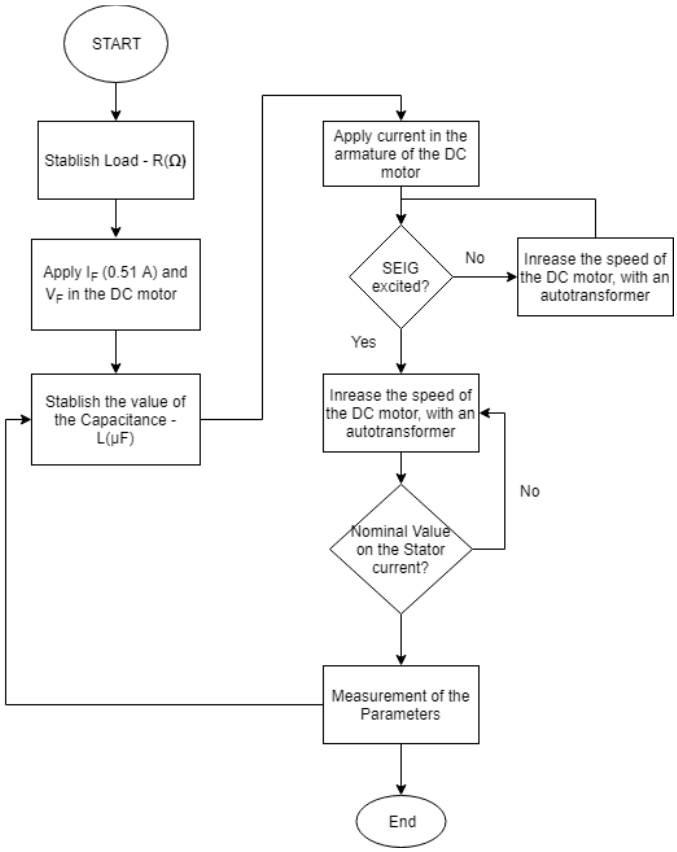

Figure 3-11 - Flowchart of the experimental tests

A diode rectifier is also necessary to convert the three-phase current to a monophasic current that feeds the armature of the DC Motor. Then, it is applied, in the system, the minimal capacitance that excites the generator. After it, the speed of the system keeps increasing until the machine gets excited and starts producing electrical power to feed the load, with recourse to the transformer. The final step of these tests is to increase the speed of the machine until the stator current in the generator reaches its nominal value of $1.6\,A$. Register all the measured values of the induction generator (the three phases of the stator voltages, V_s, the three phases of the stator current, I_s, the three phases of the active power, P_s, the three phases of the power factor, $\cos\varphi$) and the rotational speed of the whole system when the SEIG gets excited and when the generator stator current reaches its nominal value. This process is repeated several times for different values of speed and capacitance.

3.3.2 Comparison between experimental and simulation results

For the comparison of both experimental and simulation values, the figures below show two curves. One with points, which represents all the experimental points measured for a given load. From these points, it was made an interpolation, which can be observed as the striped curve in Figure 3.12 to Figure 3.14. They were also compared with the simulation values from this work, which is the interpolated curve without marks.

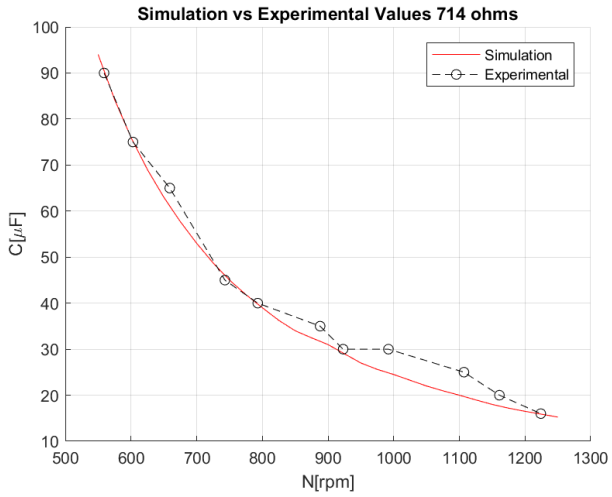

Figure 3-12 - Simulation vs Experimental values for R = 714Ω

By looking at these results it is clear to see that this SEIG model has a better performance for higher resistances. In all three cases it is shown that, once again, the speed of the generator is highly influenced by its excitation, which it depends on the load. For higher values of load resistance, the capacitance required presented smaller variations for the same speed.

Concluding, this simulation method presented small differences of results with the experimental case and the general behavior of the SEIG was equal on all simulations performed

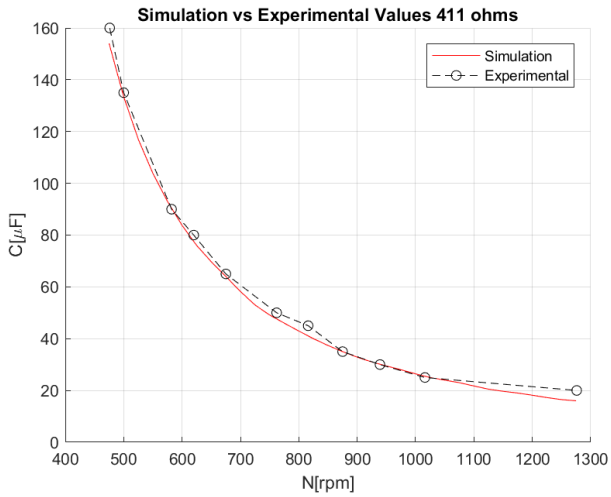

Figure 3-13 - Simulation vs Experimental values for R=411Ω

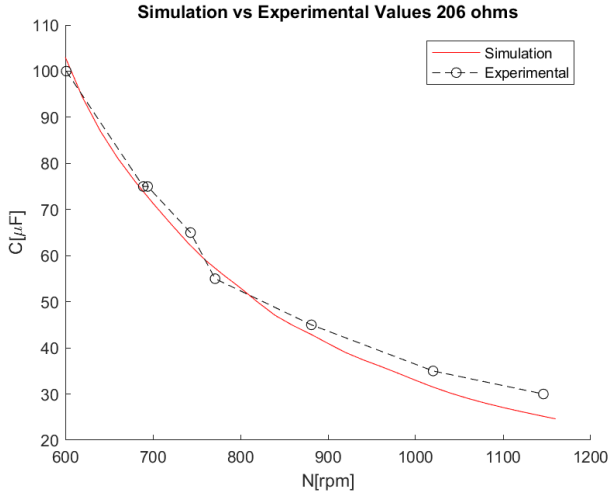

Figure 3-14 Simulation vs Experimental values for R=206Ω

4. Conclusions

The study of the application of system SEIG + PAT has increased over the years, as it was discovered the PAT is a considerably cheaper alternative for recovering energy. Electrical and Hydraulic regulation modes are the two designs which were given the biggest study throughout the years, both of them applied in a system connected to the electrical grid. In this work, it was invested some time in an off-grid approach, by isolating the system from the grid. It is a study of great interest for applications in countries where the national electrical grid is underdeveloped as this can be cheaper and a more reliable source of energy for populations with fewer possibilities. This work was intended to analyze a specific SEIG system, further to be applied in a PAT to be studied. This work was divided into two parts: Study the behavior of the induction machine parameters with frequency and voltage and a SEIG analysis.

Concerning the behavior of the induction machine, the research establishes the influence of the capacitor values to SEIG on the overall system operation points regarding non-normal conditions which is non-regulated voltage and frequency. From previous studies, the lack of accuracy of analytical models based on electrical equivalent circuit of the SEIG was verified when considering fixed electrical parameters and neglecting the iron losses or the magnetic inductance. This analysis demonstrated that it is important to develop more accurate analytical models when the pumps working as turbines are installed in water systems and they are off-grid.

Regarding the SEIG analysis, the analysis performed in this thesis showed better results from previous studies when the variation of the SEIG electrical parameters were not considered as a function of the electrical frequency and applied voltage and also when the iron losses were not considered in the model. For this analysis to occur an analytical and simulation model were made with the attention of non-fixed parameters of the induction generator. From experimental tests, all the parameters had high oscillation for different speed and loads. Both R_m and L_m parameters mainly depend on the magnetic flux. It was seen that with this new approach, both analytical and simulation model have a better accuracy when compared with the experimental results.

5. References

Capelo, B. et al. (2017) 'Electrical behaviour of the pump working as turbine in o ff grid operation', Applied Energy. Elsevier, (September), pp. 0–1. doi: 10.1016/j.apenergy.2017.10.039.

Capelo, B. (2017) Energy Recovery in Water Distribution Systems by a Pump Running as Turbine (PAT) – Grid Isolated Case. Instituto Superior Técnico, Universidade de Lisboa.

Fernandes, J. F. P. et al. (2018) 'Optimal Energy Efficiency of Isolated PAT systems by SEIG Excitation Tuning', pp. 1–26.

Kishore, A. and Kumar, G. S. (2006) 'Dynamic modeling and analysis of three phase self-excited induction generator using generalized state-space approach', International Symposium on Power Electronics, Electrical Drives, Automation and Motion, pp. 1459–1466.

Paiva, J. P. S. (2011) Redes de Energia Elétrica - Uma análise sistemática. 3a. IST Press.